





RESEARCH ARTICLE

Gapped Gaussian smoothing technique for debonding assessment with automatic thresholding

Viviana Meruane^{1,3}  | Ignacio Fernandez¹ | Rafael O. Ruiz²  | Giuseppe Petrone⁴  | Enrique Lopez-Droguett¹ 

¹Department of Mechanical Engineering, Universidad de Chile, Santiago, Chile

²Department of Civil Engineering, Universidad de Chile, Santiago, Chile

³Millennium Nucleus on Smart Soft Mechanical Metamaterials, Santiago, Chile

⁴Department of Industrial Engineering, Aerospace Section, Università degli Studi di Napoli "Federico II", Naples, Italy

Correspondence

Viviana Meruane, Department of Mechanical Engineering, Universidad de Chile, Beauchef 851, Santiago, Chile.
Email: meruane@uchile.cl

Funding information

Millennium Science Initiative of the Ministry of Economy, Development and Tourism, Grant/Award Number: Millennium Nucleus on Smart Soft Mechanical Metamaterials; Chilean National Fund for Scientific and Technological Development (FONDECYT), Grant/Award Number: 1170535

Summary

Sandwich structures are subjected to imperfect bonding or debonding caused by defects during the manufacturing process, by fatigue, or by impact loads. In this context, their safety and functionality can be improved with the implementation of vibration-based structural damage assessment methodologies. These methodologies involve the computation of second or higher order displacement derivatives, which are often obtained using the central difference method. Nevertheless, this method propagates and amplifies the measurement errors and noise. Therefore, a Gaussian process (GP) regression model to build smoothed (noise-free) curvature mode shapes from noisy experimental mode shape displacements is presented in this paper. The proposed baseline-free debonding assessment approach combines the gapped smoothing (GS) method, curvature mode shapes estimated using a GP regression, and the valley-emphasis method to automatically find damaged regions. Experimental results indicate that our approach performs better than the conventional GS method in the presence of experimental noise.

KEYWORDS

debonding, gapped smoothing, Gaussian process, sandwich panel, valley-emphasis method

1 | INTRODUCTION

Sandwich structures have become very popular in recent years mainly due to their low weight and high stiffness. Nevertheless, these structures are subjected to imperfect bonding or debonding caused by defects during the manufacturing process, by fatigue, or by impact loads.¹ This type of damage may severely deteriorate the mechanical properties of sandwich structures and could ultimately lead to a catastrophic failure.

The functionality and safety of these systems can be improved with the use of structural damage assessment methodologies, which are employed to identify any damage before it becomes a failure. Among the different methodologies to assess damage, vibration-based methods have become very popular in the past few years.² Modifications to the mechanical properties of a structure caused by damage lead to detectable variations in the vibrational properties. Therefore, by monitoring the vibrational properties, such as the resonant frequencies, mode shape displacements, modal damping, and the frequency response functions, it is possible to identify the damage.

Different response parameters have been employed to assess damage in plate-like structures based on their vibration properties. The modal strain energy (MSE) was applied by Cornwell et al.³ to localize damage in plate structures; the strain energy of the plate in damaged and undamaged conditions is used to build the damage indices. Li et al.⁴ presented

two damage indices derived from a strain mode technique to characterize damage of 2D structures: a residual strain mode shape index and a bending moment index. The variations in the uniform load surface curvature were employed by Wu and Law to localize damage in plate structures.^{5,6} Moreno-García et al.⁷ studied the performance of high-order mode shape derivatives in damage localization of 2D structures. They concluded that the fourth-order derivative provides better results.

The previous methods help identify damage by comparing the measured characteristics from damaged and undamaged structures. Therefore, reference data from an undamaged structure are a prerequisite, and pairing the damaged and undamaged modes is necessary. In some cases, useful damaged modes might not be used because they would not have been paired with the undamaged ones. To solve this problem, new types of baseline-free damage assessment algorithms have been proposed, among which gapped smoothing (GS) and wavelet-based approach stand out. Yoon et al.⁸ implemented a reference-free algorithm that uses mode shape curvatures and the GS method to identify damage in plate-like structures. Qiao et al.⁹ implemented three experimental methodologies to identify damage in composite laminates: generalized fractal dimension, MSE, and GS. Their results show that the GS method outperforms the others in identifying the delamination of the composite plate. Rucevskis et al.¹¹ proposed a damage detection algorithm for plates that uses the same principle as the GS method. In their algorithm, the damage index is computed as the difference between the measured curvature of the damaged panel and the smoothed polynomial representing the undamaged case. Chang and Chen¹⁰ developed a damage detection algorithm for plates using the spatial wavelet technique. The mode shape wavelet coefficients, computed by a one-dimensional continuous wavelet transform (CWT), are used to identify local variations due to damage. Douka et al.¹² applied the one-dimensional CWT with different wavelets to detect cracks in plates. Different investigations have implemented a 2D CWT to identify damage in 2D structures.¹²⁻¹⁵ Katunin¹⁶ introduced a damaged localization technique that uses B-splines wavelets along with the discrete wavelet transform. He demonstrated that compared with CWT approaches, their approach yields better results with lower computational times. Katunin¹⁷ focused on finding the best wavelet parameters selection, whereas in his other study,¹⁸ damage was localized in a sandwich composite panel using a fractional discrete wavelet transform.

According to Moreno-García et al.⁷ and Rucevskis et al.,¹¹ damage localization is more effective when more degrees of freedom are measured. A large arrangement of triaxial accelerometers or a scanning laser vibrometer (SLV) are usual methods for full-field vibration measurements. Nonetheless, in the first case, the structure is affected by the mass added by the accelerometers, and the number of available accelerometers restricts the number of measurement locations. On the other hand, SLVs can be used to obtain 3D data at several points, but only asynchronous measurements can be made. Furthermore, the presence of large rigid-body motions affects the SLV performance. In the last few years, the high-speed 3D digital image correlation (DIC) technique has emerged as an attractive technique for full-field vibration measurements.¹⁹ This technique determines the geometry and displacement of an object with the use of a pair of high-speed cameras, allowing to measure the displacement of thousands of points in a very short time. Seguel and Meruane²⁰ were the first to investigate the application of 3D DIC measurements in debonding assessment of sandwich composite panels, demonstrating that a high-speed 3D system can be employed effectively to locate damage in sandwich panels. Meruane et al.²¹ implemented a damage localization and quantification algorithm for composite panels that uses a linear approximation with a maximum entropy algorithm and damage indices obtained from the MSE method. The panel vibration mode shapes were measured with the use of a high-speed 3D DIC system.

The aforementioned damage assessment methods involve the computation of second or higher-order displacement derivatives, which are often obtained using the central difference method. Nevertheless, this method propagates and amplifies the measurement noise and error present in the experimental data. To solve this problem, Moreno-García et al.⁷ developed a methodology that determines the best spatial sampling based on the minimization of the total numerical differentiation error. Wu and Law⁵ followed a different approach to reduce the effect of noise. They proposed a new methodology to compute the derivatives based on a Chebyshev polynomial approximation instead of the central difference formulation. Cao et al.²² adopted a Laplacian of Gaussian filter to remove experimental noise from the mode shape displacements before using a central differences formulation to estimate the mode shape curvatures.

In the field of strain estimation based on DIC measurements, there has been recent progress in methodologies to reduce experimental noise in displacement data (smoothing techniques). Smoothing techniques are generally classified as parametric or nonparametric. In the parametric methods, it is necessary to select analytical functions that characterize the data; some examples of parametric functions used to smoothen the experimental data are the radial basis²³ and finite element shape³³ functions. In the nonparametric case, it is not necessary to make assumptions about the data; the most frequently used approach is based on least squares.³⁴ Recently, researchers have introduced a nonparametric

approach based on Gaussian process (GP) regression models.²⁵ This powerful nonparametric technique can be used to build regressions from training data.²⁶ Herein, it is demonstrated that this technique can be used to build smoothed (noise-free) curvature mode shapes from noisy experimental mode shape displacements.

Once the damage indices have been computed, it is important to define the range of damage index values corresponding to damaged and nondamaged states. A statistical approach has been proposed for damage assessment.^{8,20} This approach assumes a normal distribution for the damage indices located in the undamaged regions. Therefore, statistically significant characteristics such as damage will appear as outliers. In the field of machine vision, automatic thresholding techniques have been widely used for defects visual inspection, among which the Otsu method has been proven to be most effective.²⁷ Ng²⁸ proposed an upgrading to the Otsu method, called the valley-emphasis method, which works with bimodal distributions. The main advantage of this method over the statistical approach is that the segmentation is made automatically, without requiring parameter selection.

This paper presents a new baseline-free damage assessment algorithm for composite sandwich panels. In this algorithm, the GS method, curvature mode shapes estimated using a GP methodology, and the valley-emphasis method are combined to automatically find damaged regions. Experimental and numerical data of sandwich panels made of aluminum skins and an aluminum honeycomb core are used to validate the algorithm. Full-field vibration measurements of the sandwich panels are acquired by means of a high-speed 3D system.

To determine the benefits of our approach over an existing method, the results obtained using the proposed approach are contrasted with those of a conventional GS method with curvatures computed via a central difference approximation, for which mode shape displacements previously smoothed by a least squares approach are used.

2 | GS METHOD

As proposed by Yoon et al.,⁸ the mode shapes are first normalized by its root mean square values, as follows:

$$\varphi_r(x_i, y_j) = \phi_r(x_i, y_j) \sqrt{\frac{N_x N_y}{\sum_{i=1}^{N_x} \sum_{j=1}^{N_y} \phi_r^2(x_i, y_j)}}, \quad (1)$$

where N_x and N_y are the numbers of grid points in the corresponding directions, and $\varphi_r(x_i, y_j)$ is the normalized r th mode shape at point (x_i, y_j) .

The mode shape curvatures can be estimated using central differences as follows:

$$\nabla^2 \varphi_r(x_i, y_j) = \frac{\varphi_r(x_{i+1}, y_j) - 2\varphi_r(x_i, y_j) + \varphi_r(x_{i-1}, y_j)}{h_x^2} + \frac{\varphi_r(x_i, y_{j+1}) - 2\varphi_r(x_i, y_j) + \varphi_r(x_i, y_{j-1})}{h_y^2}, \quad (2)$$

where h_x and h_y are the grid spacings in the x and y directions, respectively. Accordingly, the undamaged mode shape curvatures can be approximated using

$$\nabla^2 \varphi_r(x_i, y_j) = \mathbf{g}_{i,j}^T \boldsymbol{\theta}_{i,j}, \quad (3)$$

where $\mathbf{g}_{i,j}$ and $\boldsymbol{\theta}_{i,j}$ correspond to a vector of base functions and their coefficients, respectively. In particular, first-order base functions are used here. This leads to

$$\mathbf{g}_{i,j}^T = [1, x_i, y_j], \quad \boldsymbol{\theta}_{i,j}^T = [a_0, a_1, a_2]. \quad (4)$$

Note that this approximation has been previously employed for similar problems.⁸ Now, Equation 3 can be arranged in matrix form by considering the neighboring points of (x_i, y_j) , as follows:

$$\boldsymbol{\lambda}_r(x_i, y_j) = \mathbf{G}_r^T(x_i, y_j) \boldsymbol{\theta}_{i,j}, \quad (5)$$

where

$$\begin{aligned}\boldsymbol{\lambda}_r^T(x_i, y_j) &= \left[\nabla^2 \varphi_r(x_{i-1}, y_{j-1}), \nabla^2 \varphi_r(x_i, y_{j-1}), \nabla^2 \varphi_r(x_{i+1}, y_{j-1}), \dots, \nabla^2 \varphi_r(x_{i+1}, y_{j+1}) \right] \\ \mathbf{G}_r^T(x_i, y_j) &= \left[\mathbf{g}_{i-1, j-1}, \mathbf{g}_{i, j-1}, \mathbf{g}_{i+1, j-1}, \dots, \mathbf{g}_{i+1, j+1} \right]\end{aligned}$$

The estimation of the parameters by least squares is given as follows:

$$\hat{\boldsymbol{\theta}}_{i,j}^r = \left(\mathbf{G}_r^T(x_i, y_j) \mathbf{G}_r(x_i, y_j) \right)^{-1} \mathbf{G}_r^T(x_i, y_j) \boldsymbol{\lambda}_r(x_i, y_j), \quad (6)$$

and the undamaged mode shape curvature is calculated as follows:

$$C_r(x_i, y_j) = \mathbf{g}_{i,j}^T \hat{\boldsymbol{\theta}}_{i,j}^r. \quad (7)$$

Ultimately, the damage indices can be calculated using

$$d_r(x_i, y_j) = \left| \nabla^2 \varphi_r(x_i, y_j) - C_r(x_i, y_j) \right|. \quad (8)$$

This expression can be expanded to consider different modes, for example, the damage index at the test point (x_i, y_j) considering m modes can be obtained using the following equation:

$$d(x_i, y_j) = \sum_{r=1}^m d_r(x_i, y_j). \quad (9)$$

3 | ESTIMATION OF CURVATURES USING GP REGRESSION

We represent the r th experimental mode shape by a set of training data $D = \langle \mathbf{X}, \boldsymbol{\phi}_r \rangle$, where $\mathbf{X} = [(x_1, y_1), (x_2, y_2), \dots, (x_n, y_n)]$ are the coordinates of the points in the grid, and $\boldsymbol{\phi}_r = [\phi_r(x_1, y_1), \phi_r(x_2, y_2), \dots, \phi_r(x_n, y_n)]$ are the mode shape displacements corresponding to each point. The observed mode shape vector is obtained from a noisy process, expressed by

$$\phi_r(x_i, y_i) = f(x_i, y_i) + \epsilon, \quad (10)$$

where ϵ corresponds to an additive Gaussian noise with zero mean and variance σ_n^2 . Given the training data $D = \langle \mathbf{X}, \boldsymbol{\phi}_r \rangle$, the GP prediction for the mean of the mode shape displacement at point (x^*, y^*) is

$$\phi_r^s(x^*, y^*) = \mathbf{k}^{*T} \mathbf{K}^{-1} \boldsymbol{\phi}_r, \quad (11)$$

where \mathbf{k}^* is a vector containing the *kernel* values between the test point (x^*, y^*) and the points in the grid \mathbf{X} and is expressed as

$$\mathbf{k}^*[i] = k((x^*, y^*), (x_i, y_i)). \quad (12)$$

The function k corresponds to the autocorrelation function of the GP. The matrix \mathbf{K} is the kernel matrix of the grid points:

$$\mathbf{K}[i, j] = k((x_i, y_i), (x_j, y_j)). \quad (13)$$

The most widely used kernel is the Gaussian kernel with additive noise:

$$k((x_i, y_i), (x_j, y_j)) = e^{-\frac{1}{2} \left(\frac{(x_i - x_j)^2}{s_x^2} + \frac{(y_i - y_j)^2}{s_y^2} \right)} + \sigma_n^2 \delta_{ij}, \quad (14)$$

where s_x^2 and s_y^2 are the length scales that reflect the relative smoothness of the process along the x and y directions, respectively. The parameter σ_n^2 accounts for the global noise of the process, and δ_{ij} corresponds to the Kronecker delta.

The smoothed mode shape displacements ϕ_r^s are estimated by evaluating Equation 11 at the grid points. The mode shape curvatures can be obtained from the analytical expression of the mode shape displacements, thus avoiding numerical differentiation. The smoothed mode shape curvatures are given by

$$\frac{\partial^2 \phi_r^s(x^*, y^*)}{\partial x^2} = [\mathbf{k}_{*xx}]^T \mathbf{K}^{-1} \phi_r, \quad (15)$$

and

$$\frac{\partial^2 \phi_r^s(x^*, y^*)}{\partial y^2} = [\mathbf{k}_{*yy}]^T \mathbf{K}^{-1} \phi_r, \quad (16)$$

where \mathbf{k}_{*xx} and \mathbf{k}_{*yy} are the vectors containing the second-order derivatives of the kernel function evaluated between the test point (x^*, y^*) and the points in the grid \mathbf{X} . The second-order derivatives of the kernel function are given by

$$\frac{\partial^2 k}{\partial x^2}((x_i, y_i), (x_j, y_j)) = \left[\left(\frac{x_i - x_j}{s_x^2} \right)^2 - \frac{1}{s_x^2} \right] k((x_i, y_i), (x_j, y_j)) \quad (17)$$

and

$$\frac{\partial^2 k}{\partial y^2}((x_i, y_i), (x_j, y_j)) = \left[\left(\frac{y_i - y_j}{s_y^2} \right)^2 - \frac{1}{s_y^2} \right] k((x_i, y_i), (x_j, y_j)). \quad (18)$$

4 | AUTOMATIC THRESHOLDING METHOD

A grayscale image can be characterized by an intensity function with a total of L levels. Automatic thresholding methods separate objects of interest with the use of threshold values, thus each family of objects is designated to a certain range of levels in the grayscale. Let us assume that the image contains a total of n pixels, and n_i corresponds to the number of pixels in level i . Therefore, the probability of level i is

$$p_i = \frac{n_i}{n}. \quad (19)$$

In the single thresholding case, the pixels are separated into two classes $C_1 = \{1, 2, \dots, q\}$ and $C_2 = \{q+1, q+2, \dots, L\}$, where q is the threshold value. The probabilities for each class are

$$P_1(q) = \sum_{i=1}^q p_i \quad \text{and} \quad P_2(q) = \sum_{i=q+1}^L p_i. \quad (20)$$

The mean levels in each class are given by

$$\mu_1 = \sum_{i=1}^q i p_i / P_1 \quad \text{and} \quad \mu_2 = \sum_{i=q+1}^L i p_i / P_2. \quad (21)$$

The valley-emphasis method maximizes the variance between the two groups while minimizing the probability of occurrence at the threshold value:

$$q^* = \operatorname{argmax}_{0 < q \leq L} \left((1 - p_q) (P_1(q) \mu_1^2 + P_2(q) \mu_2^2) \right). \quad (22)$$

5 | PROPOSED APPROACH

The proposed approach comprises the next steps:

1. Obtain the experimental mode shape displacements and normalize them by their root mean square values according to Equation 1.

2. Select the length scale parameter s_x^2 and the noise variance σ_n^2 and estimate the smooth mode shape curvatures using the procedure described in Section 3. As the grid size is the same in the x and y directions, the parameter s_y^2 is set equal to s_x^2 .
3. Compute the damage indices following Equations 3–9.
4. Identify the damaged region using the automatic thresholding method described in Section 4.

The results of the proposed approach were compared with those of conventional GS methods with curvatures computed via the central difference approximation, for which the mode shape displacements previously smoothed by a least squares approach were employed. The algorithm consists of the next steps:

1. Obtain the experimental mode shape displacements and smooth them using a penalized least squares method via discrete cosine transform²⁹ (one parameter needs to be selected).
2. Compute the damage indices as explained in Section 2 (Equations 1–9).
3. Identify the damaged region using the automatic thresholding method described in Section 4.

The performances of the two approaches were evaluated in terms of the intersection over union (IoU) metric, which has been widely used to evaluate object detection and image segmentation algorithms.³⁰ For damage identification, this metric was computed by dividing the area of overlap between the predicted and true damaged regions by the area of the union of the two regions (see Figure 1) and is expressed as follows:

$$IoU = \frac{\text{Area of overlap}}{\text{Area of union}} = \frac{TP}{TP + FP + FN}, \quad (23)$$

where TP , FN , and FP are the true positives, false negatives, and false positives, respectively.

6 | APPLICATION CASE

The application case presented in Figure 2 is an aluminum sandwich panel with a honeycomb core. One of the skins is painted with a speckle pattern, which is necessary for the DIC measurements. The dimensions of the panel are $0.35 \text{ m} \times 0.25 \text{ m} \times 0.021 \text{ m}$. The characteristics of the skins and core are presented in Tables 1 and 2.

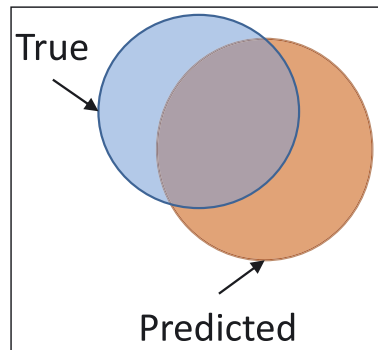


FIGURE 1 Scheme of predicted and true damaged regions



FIGURE 2 Aluminum sandwich with the speckle pattern

TABLE 1 Characteristics of the skin

Thickness	0.8 mm
Elastic modulus	6.9×10^{10} Pa
Poisson's ratio	0.33
Density	2,700 kg/m ³

TABLE 2 Characteristics of the aluminum honeycomb core

Cell size	19.1 mm
Foil thickness	5×10^{-5} m
Thickness	10 mm
Density	20.8 kg/m ³
Compressive strength	0.448 MPa
Longitudinal shear strength (σ_{xy})	0.345 MPa
Longitudinal shear modulus (G_{xy})	89.63 MPa
Transversal shear strength (σ_{yz})	0.241 MPa
Transversal shear modulus (G_{yz})	41.37 MPa

The aluminum honeycomb core is joined to the two skins by means of an epoxy resin that cures at ambient temperature and can be used for bonding aluminum to a variety of materials. Figure 3a presents one of the aluminum skins with a layer of epoxy resin, in this case debonding is introduced as a circular region without adhesive. Figure 3b shows the vacuum bagging system used during curing to ensure a perfect bonding.

Panels with four different damage scenarios were built, as shown in Figure 4. The damage is characterized by circular and square shapes with normalized sizes varying between 0.07 and 0.17. Table 3 lists a summary of the damage scenarios with dimensions. In Cases 3 and 4, there are two debonded regions in the panel.

6.1 | Numerical results

The performances of the damage assessment algorithms were first evaluated using a finite element model of the panel, which was first built in Meruane et al.³¹ A three-layer shell model represents the honeycomb sandwich panel; the skins

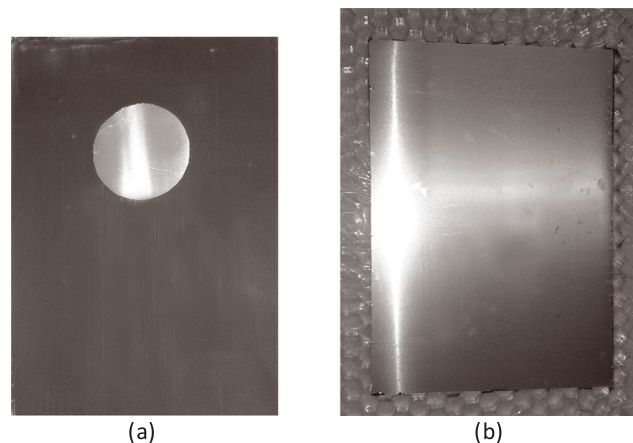


FIGURE 3 Manufacturing of experimental panel: (a) layer of epoxy resin over the skin, the circle without adhesive corresponds to the debonded region, and (b) vacuum bagging curing

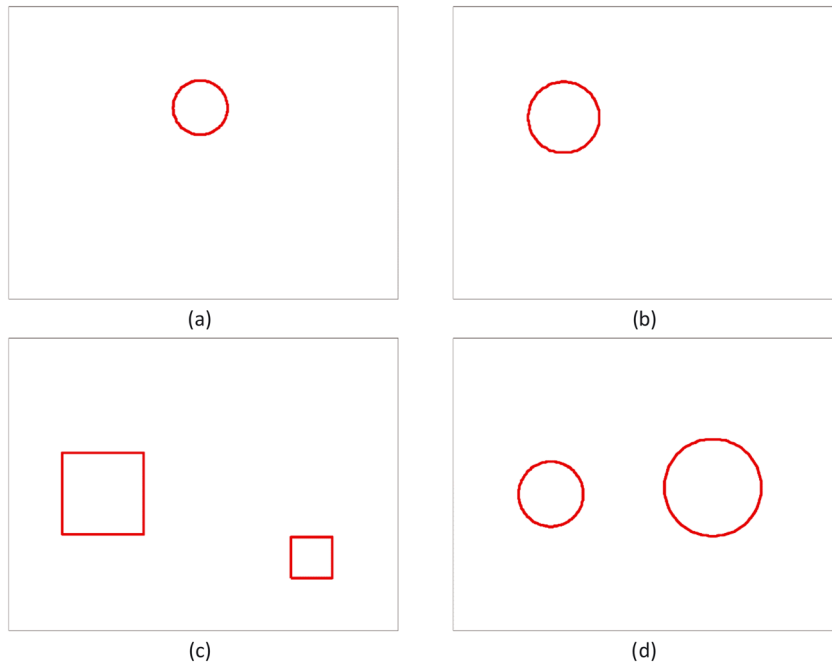


FIGURE 4 Scheme of the debonded regions introduced to the experimental panels, which are indicated by the red lines

TABLE 3 Damage scenarios introduced to the experimental panels

Case	Normalized damage size		Shape
	Damage 1	Damage 2	
1	0.09	—	Circular
2	0.12	—	Circular
3	0.14	0.07	Square
4	0.11	0.17	Circular

and the core are connected through linear springs that represent the epoxy adhesive layer. As illustrated in Figure 5, debonding damage is introduced by reducing the stiffness of the springs in that zone.

The finite element model, which is shown in Figure 6, was built with the Structural Dynamics Toolbox³² of MATLAB®. Standard isotropic four-node shell element were used to model the skins and honeycomb core.

The numerical mode shapes were polluted with 10% random noise to simulate experimental measurements. As an example, the first three mode shapes of an undamaged panel are illustrated in Figure 7. A database with 500 damage scenarios is created to evaluate the damage assessment algorithms. The debonded regions have circular shapes and are placed randomly throughout the panel with random diameters ranging between 1 and 10 cm.

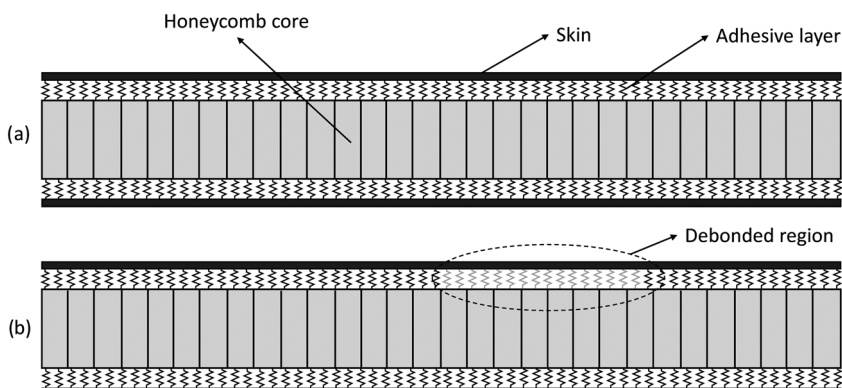


FIGURE 5 Side view of the numerical panel: (a) undamaged and (b) with a debonded region

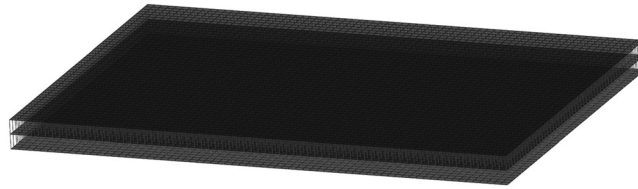


FIGURE 6 Three-layer shell model representing the sandwich panel

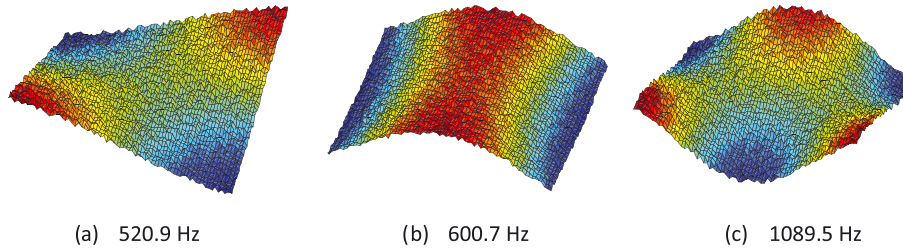


FIGURE 7 First three undamaged numerical mode shapes with 10% random noise

The performance of the proposed damage assessment methodology was evaluated as a function of the length scale parameter s_x and the noise variance σ_n^2 . The length scale parameter was varied between $4d_x$ and $7d_x$, where d_x is the distance between the two points on the grid. The results, shown in Figure 8, confirm that the best combination of parameters is $s_x = 5d_x$ and $\sigma_n^2 = 1$, which will be used hereinafter.

In the case of the conventional GS method with curvatures computed using a central difference approximation, the only parameter to be selected is the smoothing factor. Figure 9 shows the performance of the conventional GS method with central differences as a function of the smoothing factor. In this case, the results are very sensitive to the smoothing

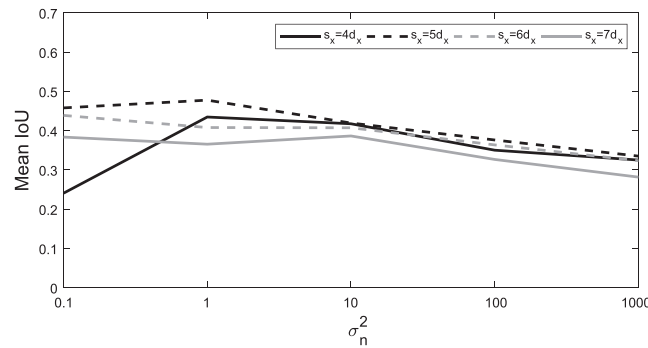


FIGURE 8 Performance of the proposed damage assessment methodology as a function of the length scale parameter s_x^2 and the noise variance σ_n^2

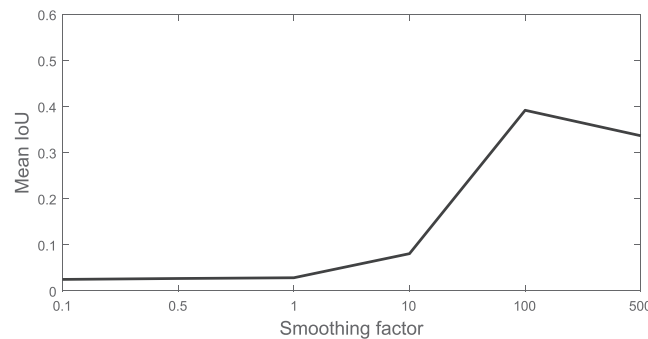


FIGURE 9 Performance of the conventional gapped smoothing (GS) with central differences as a function of the smoothing factor

factor. The best results are obtained with a factor of 100. When a lower factor is used, the performance decreases drastically. In the subsequent implementations of this algorithm, a smoothing factor of 100 is used.

The panels in the database were categorized into five groups according to their size, and the mean performance indicator IoU was calculated for each group. Figure 10 shows the results. In all the cases, the proposed Gaussian-based algorithm outperforms the method based on the central differences. Regarding the damage size, both algorithms cannot identify the damage when the normalized size is lower than 0.05 and are ineffective when the damage size is lower than 0.1 or higher than 0.2. The best performance is obtained for normalized damage sizes in the range [0.15–0.2].

Figures 11 and 12 show some examples of damage identified using the conventional GS method with central difference approximation and the proposed approach, respectively. The images on the left show the damage indices, and those on the right show the damage detected using the automatic threshold algorithm. The red circles/squares indicate the true damage.

In the three examples presented in Figures 11 and 12, the GS method with the central difference approximation exhibits a large background noise, whereas the proposed algorithm significantly reduces the effects of noise. Although in Figure 10, the difference in the mean IoU between both algorithms is not much, it is clear from the damage indices

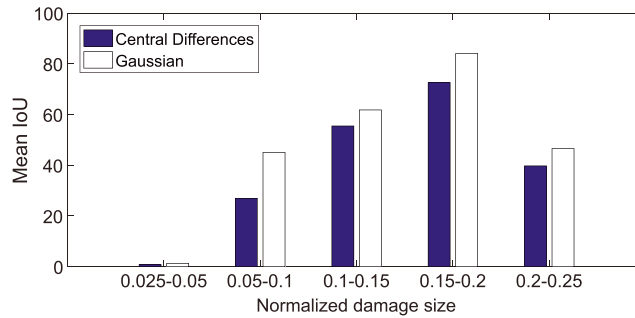


FIGURE 10 Damage assessment performance as a function of the normalized damage size

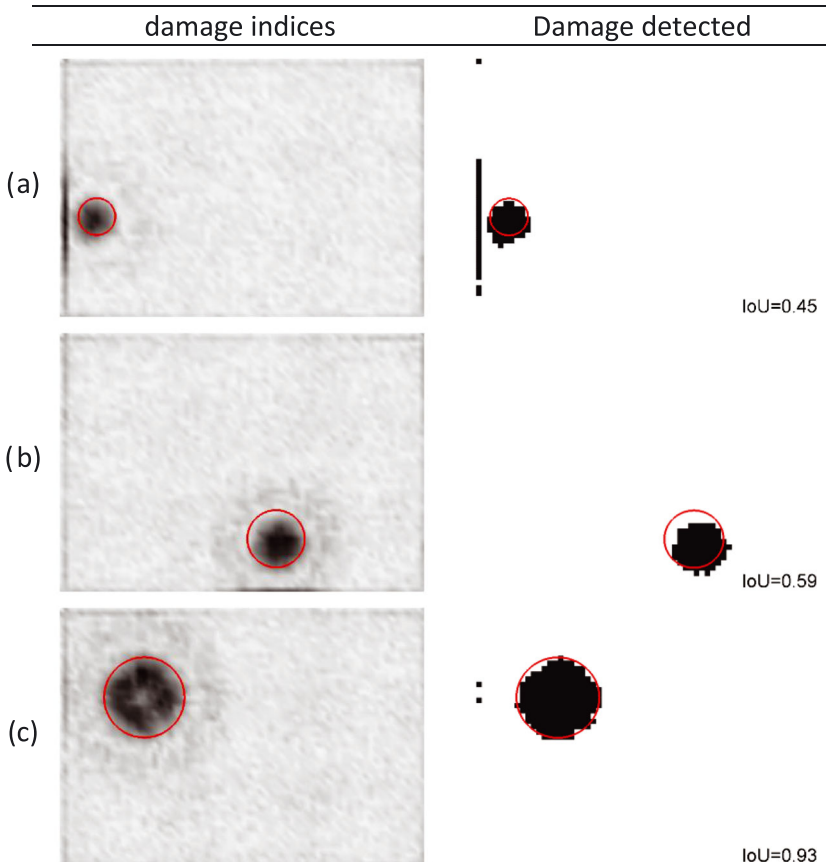


FIGURE 11 Damage identified using the gapped smoothing (GS) method with central difference approximation. Normalized damage sizes: (a) 0.08, (b) 0.12, and (c) 0.17

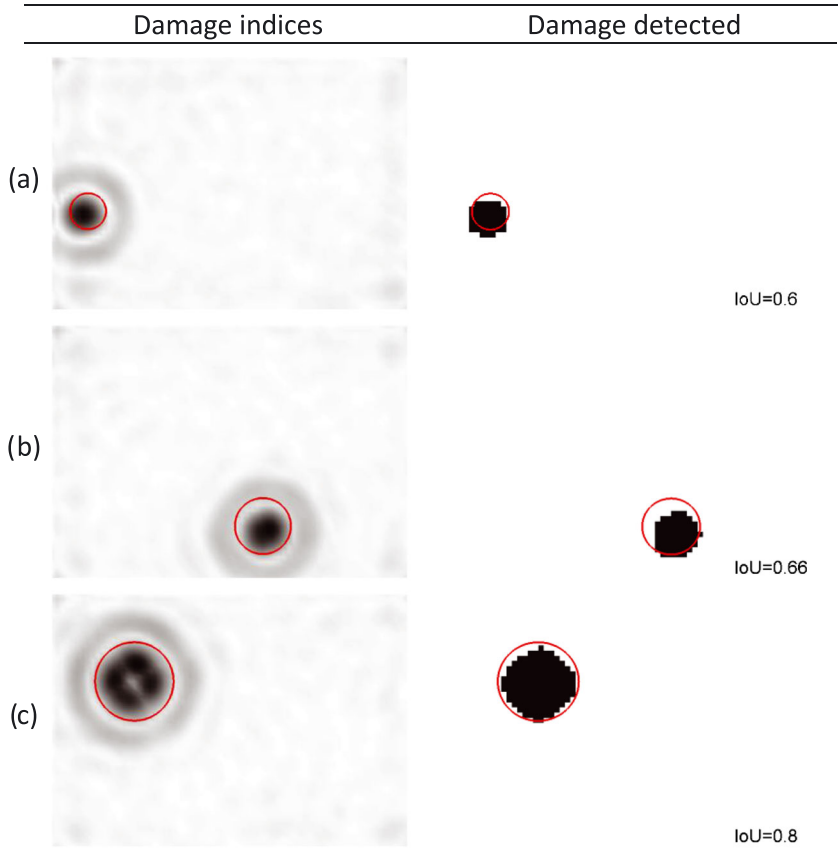


FIGURE 12 Damage identified using the proposed approach. Normalized damage sizes: (a) 0.08, (b) 0.12, and (c) 0.17

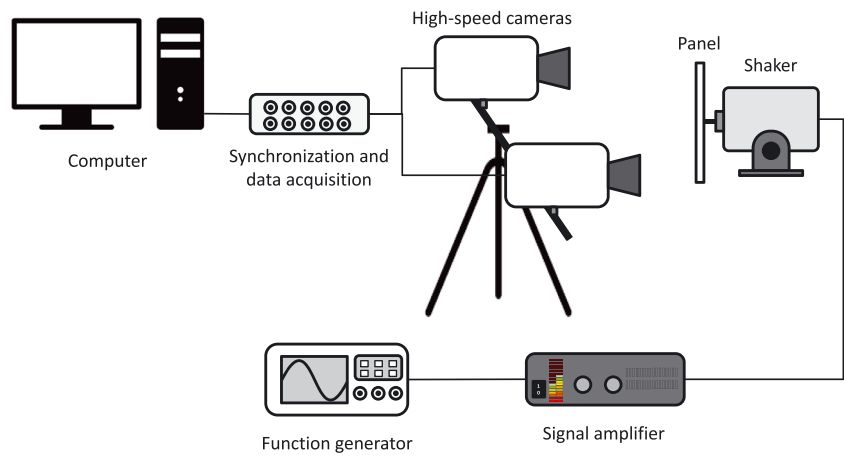


FIGURE 13 Schematic of the experimental setup

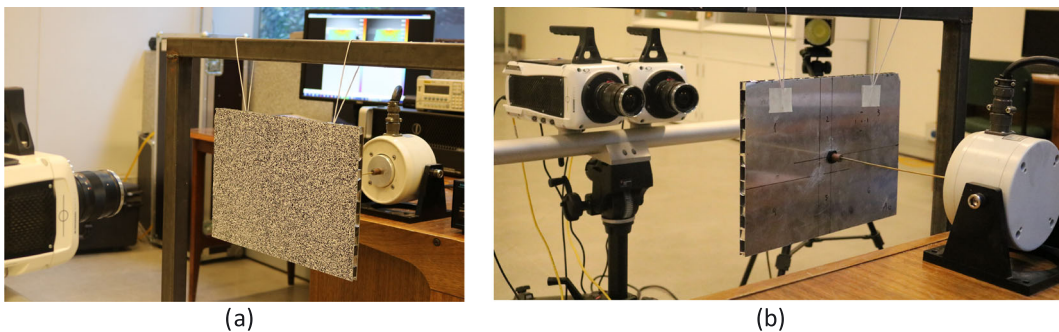


FIGURE 14 Experimental setup: (a) front view showing the panel with the speckle pattern, (b) back view showing the shaker attachment

that the proposed method is less sensitive to the experimental noise and almost does not detect false damage, whereas the conventional method based on central differences tends to detect false damage due to the experimental noise.

6.2 | Experimental results

Figure 13 shows the schematic of the experimental setup. Soft springs hang the panel to represent a “free–free” boundary condition, which is driven by an electrodynamic shaker. Two high-speed synchronized cameras connected to the DIC software capture the panel displacements. The DIC system consists of the Q450 high-speed DIC system

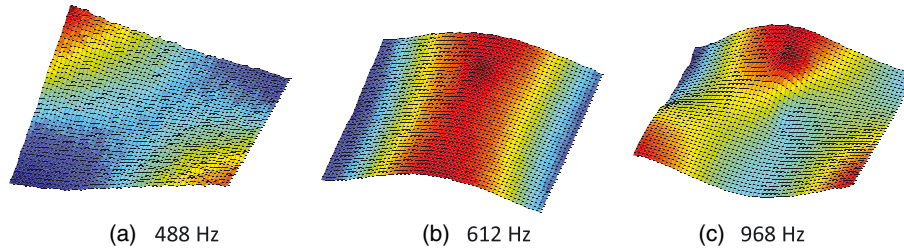


FIGURE 15 First three experimental mode shapes identified for Case 1

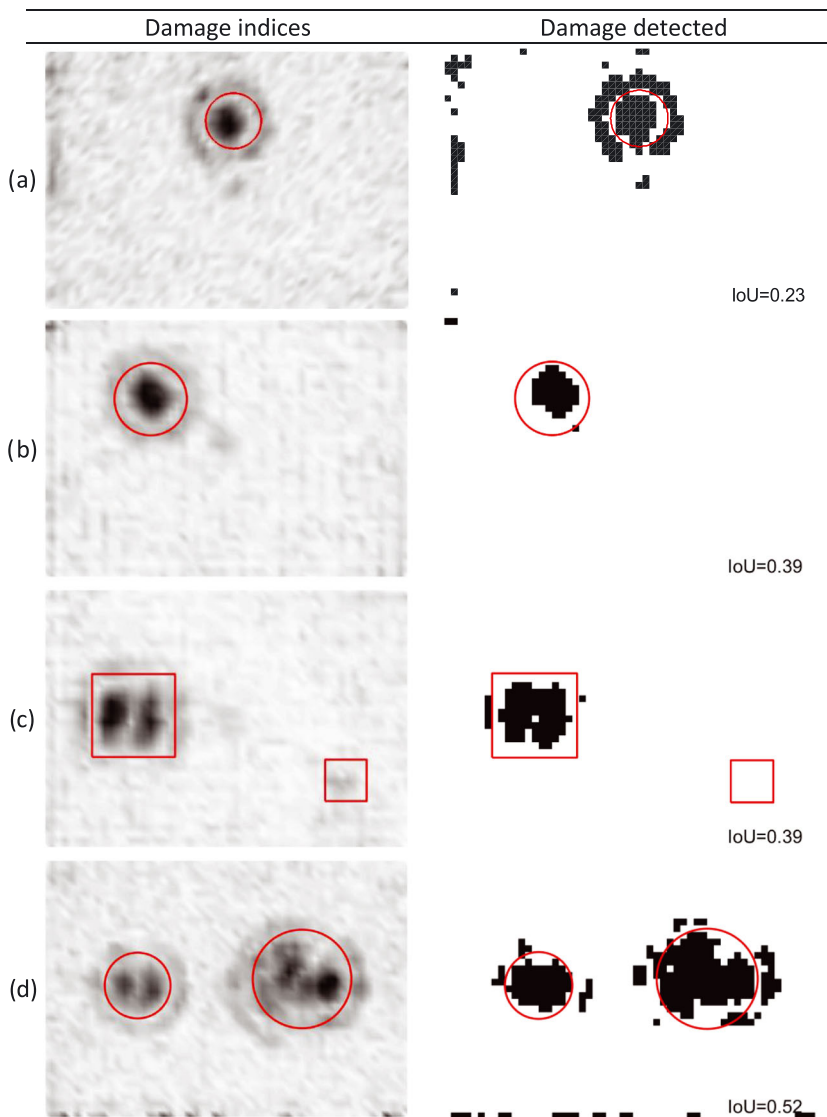


FIGURE 16 Experimental damage identified using the gapped smoothing (GS) method with central difference approximation. Normalized damage sizes: (a) 0.09, (b) 0.12, (c) 0.14 and 0.07, and (d) 0.11 and 0.17

manufactured by Dantec Dynamics, which is composed by the cameras, data acquisition, and DIC software. The maximum acquisition frequency at a resolution of 1 MP is 7,530 fps. The actual experimental setup is shown in Figure 14, where front and back views of the panel are presented.

The procedure to identify the experimental modes shapes is described in Seguel and Meruane²⁰ and can be summarized as follows:

1. Identify the panel natural frequencies from an impact test.
2. Add a speckle pattern to the panel.
3. Tune the shaker to the natural frequency and excite the panel.
4. Record the panel vibration with high-speed cameras and determine the displacements using a DIC software.
5. Export the displacements to MATLAB, estimate the operational mode shape, and smoothen it.
6. Select another natural frequency and go to step 3.

For each panel, all the mode shapes in the frequency range of 1–2,000 Hz were identified. The number of identified modes is between 6 and 11, depending on the panel. As an example, Figure 15 shows the first three modes identified for the first panel (Case 1).

Figures 16 and 17 show the damage identification results obtained using the GS method with central difference approximation and the proposed approach, respectively. The images on the left show the damage indices, and those on the right show the damage detected using the automatic threshold algorithm. The red circles/squares indicate the

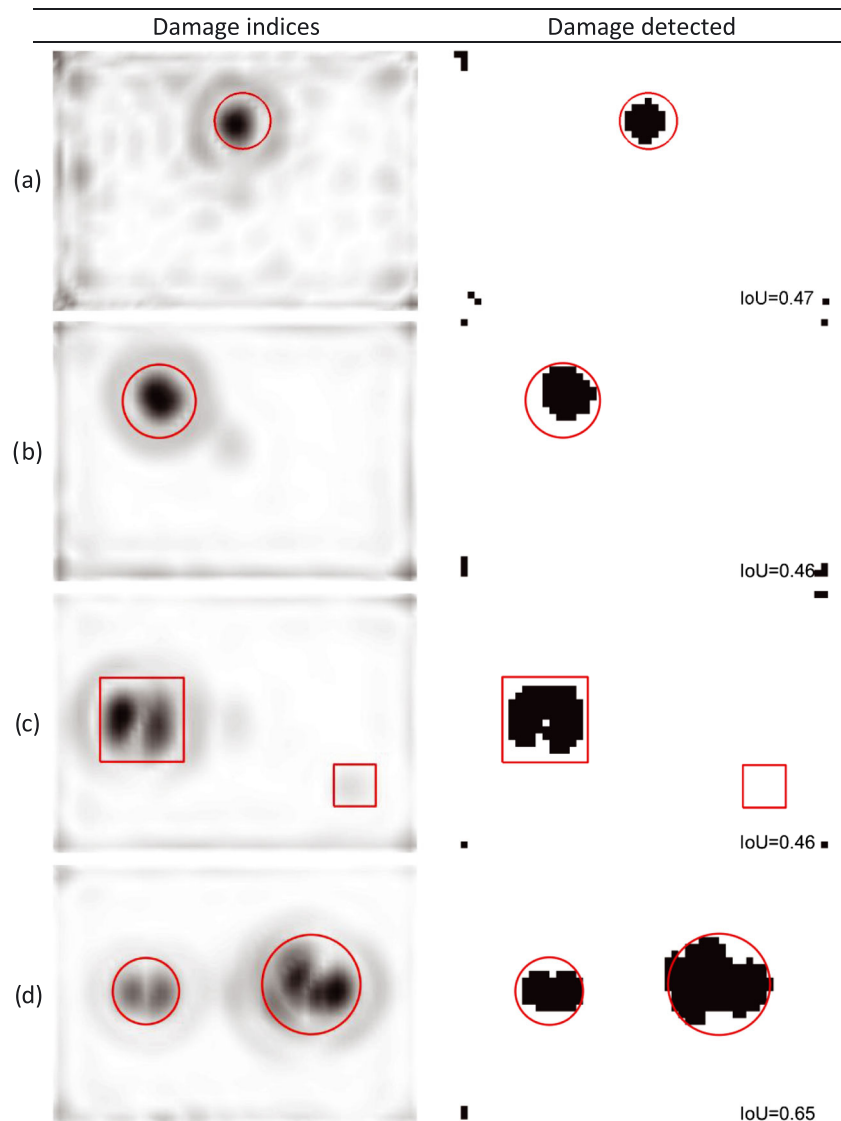


FIGURE 17 Experimental damage identified using the proposed approach. Normalized damage sizes: (a) 0.09, (b) 0.12, (c) 0.14 and 0.07, and (d) 0.11 and 0.17

TABLE 4 Performance of the algorithms for the experimental panels

Case	IoU	
	GS with central difference approximation	Proposed approach
1	0.23	0.47
2	0.39	0.46
3	0.39	0.46
4	0.52	0.65

Abbreviations: GS, gapped smoothing; IoU, intersection over union.

true damage. In the four cases, the proposed approach outperforms the existing method, proving to be more robust to experimental noise. Table 4 summarizes the performance of the two algorithms.

The results, shown in Figures 16 and 17, confirm that both algorithms fail to detect the smaller damage in Case 3, wherein the normalized size is 0.07, whereas they correctly identify the damage in Case 1, wherein the normalized size is 0.09. Damage scenarios with a normalized size lower than 0.08 are not well identified. This was expected, as it was demonstrated in the numerical analysis that the algorithms are ineffective when it comes to identifying small damage.

7 | CONCLUSIONS

A new baseline-free algorithm to assess the damage in composite sandwich panels was proposed in this paper. In the proposed algorithm, the GS method, curvature mode shapes estimated using a GP methodology, and valley-emphasis method are combined to automatically find damage regions. The algorithm was applied to assess the debonding of sandwich composite panels made of aluminum skins and an aluminum honeycomb core using high-speed DIC measurements. Further, the numerical and experimental results were compared with those of a conventional GS approach, wherein the central difference approximation is employed to compute mode shape curvatures.

The results show that the conventional method is more sensitive to experimental noise because the curvatures are calculated using the central difference approximation, which amplifies the experimental noise. In contrast, the proposed approach identifies the damage more clearly and is not affected by experimental noise, as the GP methodology implemented to estimate the curvatures was found to be robust against experimental noise. As such, the proposed approach is more suitable for damage identification in the presence of experimental noise.

Both algorithms fail to identify damage with a normalized size lower than 0.08. This is related to the sensitivity of the curvature modes shapes to small damage. Therefore, the proposed approach can be used to identify moderate to large damage with a normalized size greater than 0.08. To identify smaller damage, local inspection methods, such as ultrasonic techniques, can be employed.

In the future, this approach will be applied to more complex and realistic structures and will be combined with deep learning models to improve the algorithm performance.

ACKNOWLEDGEMENTS

This work was supported by the Chilean National Fund for Scientific and Technological Development (FONDECYT) (grant 1170535) and the Millennium Science Initiative of the Ministry of Economy, Development and Tourism grant “Millennium Nucleus on Smart Soft Mechanical Metamaterials.”

ORCID

Viviana Meruane  <https://orcid.org/0000-0002-6692-2687>

Rafael O. Ruiz  <https://orcid.org/0000-0002-5721-9674>

Giuseppe Petrone  <https://orcid.org/0000-0002-5275-5531>

Enrique Lopez-Droguett  <https://orcid.org/0000-0002-0790-8439>

REFERENCES

1. Tomblin J, Lacy T, Smith B, Hooper S, Vizzini A. Review of damage tolerance for composite sandwich airframe structures. WICHITA STATE UNIV KS; 1999.
2. Carden EP, Fanning P. Vibration based condition monitoring: a review. *Struct Heal Monit*. 2004;3(4):355-377.
3. Cornwell P, Doebling SW, Farrar CR. Application of the strain energy damage detection method to plate-like structures. *J Sound Vib*. 1999;224(2):359-374.
4. Li YY, Cheng L, Yam LH, Wong WO. Identification of damage locations for plate-like structures using damage sensitive indices: strain modal approach. *Compos Struct*. 2002;80(25):1881-1894.
5. Wu D, Law SS. Damage localization in plate structures from uniform load surface curvature. *J Sound Vib*. 2004;276(1-2):227-244.
6. Wu D, Law SS. Sensitivity of uniform load surface curvature for damage identification in plate structures. *J Vib Acoust*. 2005;127(1):84-92.
7. Moreno-García P, dos Santos JVA, Lopes H. A new technique to optimize the use of mode shape derivatives to localize damage in laminated composite plates. *Compos Struct*. 2014;108:548-554.
8. Yoon MK, Heider D, Gillespie JW, Ratcliffe CP, Crane RM. Local damage detection using the two-dimensional gapped smoothing method. *J Sound Vib*. 2005;279(1-2):119-139.
9. Qiao P, Lu K, Lestari W, Wang J. Curvature mode shape-based damage detection in composite laminated plates. *Compos Struct*. 2007;80(3):409-428.
10. Chang CC, Chen LW. Damage detection of a rectangular plate by spatial wavelet based approach. *Appl Acoust*. 2004;65(8):819-832.
11. Rucevskis S, Janeliukstis R, Akishin P, Chate A. Mode shape-based damage detection in plate structure without baseline data. *Struct Control Health Monit*. 2016;23(9):1180-1193.
12. Douka E, Loutridis S, Trochidis A. Crack identification in plates using wavelet analysis. *J Sound Vib*. 2004;270(1-2):279-295.
13. Rucka M, Wilde K. Application of continuous wavelet transform in vibration based damage detection method for beams and plates. *J Sound Vib*. 2006;297(3-5):536-550.
14. Huang Y, Meyer D, Nemat-Nasser S. Damage detection with spatially distributed 2D continuous wavelet transform. *Mech Mater*. 2009;41(10):1096-1107.
15. Fan W, Qiao P. A 2-D continuous wavelet transform of mode shape data for damage detection of plate structures. *Int J Solids Struct*. 2009;46(25-26):4379-4395.
16. Katunin A. Damage identification in composite plates using two-dimensional B-spline wavelets. *Mech Syst Signal Process*. 2011;25(8):3153-3167.
17. Katunin A. Stone impact damage identification in composite plates using modal data and quincunx wavelet analysis. *Arch Civil Mech Eng*. 2015;15(1):251-261.
18. Katunin A. Vibration-based spatial damage identification in honeycomb-core sandwich composite structures using wavelet analysis. *Compos Struct*. 2014;118:385-391.
19. Helfrick MN, Niezrecki C, Avitabile P, Schmidt T. 3D digital image correlation methods for full-field vibration measurement. *Mech Syst Signal Process*. 2011;25(3):917-927.
20. Seguel F, Meruane V. Damage assessment in a sandwich panel based on full-field vibration measurements. *J Sound Vib*. 2018;417:1-18.
21. Meruane V, Lasen M, Droguett EL, Ortiz-Bernardin A. Modal strain energy-based debonding assessment of sandwich panels using a linear approximation with maximum entropy. *Entropy*. 2017;19(11):619.
22. Cao S, Ouyang H, Cheng L. Baseline-free multidamage identification in plate-like structures by using multiscale approach and low-rank modelling. *Struct Control Health Monit*. 2019;26(2):e2293.
23. Dai X, Yang F, Chen Z, Shao X, He X. Strain field estimation based on digital image correlation and radial basis function. *Opt Lasers Eng*. 2015;65:64-72.
24. Meng LB, Jin GC, Yao XF. Application of iteration and finite element smoothing technique for displacement and strain measurement of digital speckle correlation. *Opt Lasers Eng*. 2007;45(1):57-63.
25. Rasmussen CE. Gaussian processes in machine learning. In: *Advanced Lectures on Machine Learning*. Berlin; 2004:63-71.
26. Ko J, Fox D. GP-BayesFilters: Bayesian filtering using Gaussian process prediction and observation models. *Auton Robots*. 2009;27(1):75-90.
27. Otsu N. A threshold selection method from gray-level histograms. *IEEE Trans Syst Man Cybern*. 1979;9(1):62-66.
28. Ng HF. Automatic thresholding for defect detection. *Pattern Recognit Lett*. 2006;27(14):1644-1649.
29. Garcia D. Robust smoothing of gridded data in one and higher dimensions with missing values. *Comput Stat Data Anal*. 2010;54(4):1167-1178.
30. Rahman MA, Wang Y. Optimizing intersection-over-union in deep neural networks for image segmentation. In: *International Symposium on Visual Computing*. Cham: Springer; 2016:234-244.
31. Meruane V, del Fierro V, Ortiz-Bernardin A. A maximum entropy approach to assess debonding in honeycomb aluminum plates. *Entropy*. 2014;16(5):2869-2889.

32. Balmès E, Bianchi JP, Leclère JM. Structural dynamics toolbox user's guide. Version; 2011.
33. Zhao J, Zeng P, Pan B, et al. Improved hermite finite element smoothing method for full-field strain measurement over arbitrary region of interest in digital image correlation. *Opt Lasers Eng.* 2012;50(11):1662-1671.
34. Pan B, Asundi A, Xie H, Gao J. Digital image correlation using iterative least squares and pointwise least squares for displacement field and strain field measurements. *Opt Lasers Eng.* 2009;47(7-8):865-874.

How to cite this article: Meruane V, Fernandez I, Ruiz RO, Petrone G, Lopez-Droguett E. Gapped Gaussian smoothing technique for debonding assessment with automatic thresholding. *Struct Control Health Monit.* 2019;26:e2371. <https://doi.org/10.1002/stc.2371>